

Miniature Implantable Antennas for Biomedical Telemetry: From Simulation to Realization

Asimina Kiourti*, *Student Member, IEEE*, Jorge R. Costa, *Senior Member, IEEE*,

Carlos A. Fernandes, *Senior Member, IEEE*, André G. Santiago, and Konstantina S. Nikita, *Senior Member, IEEE*

Abstract—We address numerical versus experimental design and testing of miniature implantable antennas for biomedical telemetry in the medical implant communications service band (402–405 MHz). A model of a novel miniature antenna is initially proposed for skin implantation, which includes varying parameters to deal with fabrication-specific details. An iterative design-and-testing methodology is further suggested to determine the parameter values that minimize deviations between numerical and experimental results. To assist *in vitro* testing, a low-cost technique is proposed for reliably measuring the electric properties of liquids without requiring commercial equipment. Validation is performed within a specific prototype fabrication/testing approach for miniature antennas. To speed up design while providing an antenna for generic skin implantation, investigations are performed inside a canonical skin-tissue model. Resonance, radiation, and safety performance of the proposed antenna is finally evaluated inside an anatomical head model. This study provides valuable insight into the design of implantable antennas, assessing the significance of fabrication-specific details in numerical simulations and uncertainties in experimental testing for miniature structures. The proposed methodology can be applied to optimize antennas for several fabrication/testing approaches and biotelemetry applications.

Index Terms—Biomedical telemetry, dielectric measurements, implantable antenna, *in vitro*, medical implant communications service (MICS) band.

I. INTRODUCTION

WIRELESS antenna telemetry for implantable biomedical devices is recently receiving considerable attention for diagnosis and therapy [1]–[5]. Bidirectional communication between the implanted device and exterior monitoring/control

Manuscript received February 14, 2012; revised April 5, 2012; accepted May 25, 2012. Date of publication; date of current version. This work was supported in part by the Fundação para a Ciência e Tecnologia, Portugal, under Project RFID Local PTDC/EEA-TEL/102390/2008. The work of A.K. was supported by the IEEE Antennas and Propagation Society Doctoral Research Award. Asterisk indicates corresponding author.

*A. Kiourti is with the School of Electrical and Computer Engineering and the Institute of Communications and Computer Systems, National Technical University of Athens, Athens 15780, Greece (e-mail: akiourti@biosim.ntua.gr).

J. R. Costa is with the Instituto de Telecomunicações and the Departamento de Ciências e Tecnologias da Informação, Instituto Universitário de Lisboa (ISCTE-IUL), Lisboa 1649-026, Portugal (e-mail: Jorge.Costa@lx.it.pt).

C. A. Fernandes is with Instituto de Telecomunicações and the Instituto Superior Técnico, Technical University of Lisbon, Lisboa 1049-001, Portugal (e-mail: carlos.fernandes@lx.it.pt).

A. G. Santiago is with Instituto Superior Técnico, Technical University of Lisbon, Lisboa 1049-001, Portugal (e-mail: andre.santiago.1988@gmail.com).

K. S. Nikita is with the School of Electrical and Computer Engineering and the Institute of Communications and Computer Systems, National Technical University of Athens, Athens 15780, Greece (e-mail: knikita@ece.ntua.gr).

Color versions of one or more of the figures in this paper are available online at <http://ieeexplore.ieee.org>.

Digital Object Identifier 10.1109/TBME.2012.2202659

equipment is most commonly performed in the medical implant communications service (MICS) band (402–405 MHz), which is regulated by the United States Federal Communications Commission [6] and the European Radiocommunications Committee [7]. Patch designs are preferred for implant-integrated antennas because of their flexibility in design, conformability, and shape [8].

Design of implantable patch antennas operating in the low-frequency MICS band draws high-scientific interest to deal with miniaturization. The aim is to decrease the antenna physical size, while increasing its electrical size. Rectangular 10 × 40- and 5760- mm^3 chest-implantable antennas have been reported [1], which use the high-permittivity ($\epsilon_r = 10.2$) Rogers 3210 dielectric and apply a spiral radiator for size reduction. Addition of a shorting pin, thus, conversion to a planar inverted-F antenna (PIFA) acts like a ground plane on a monopole, and has been found to shrink the volume of the aforementioned antennas by 40% and 60%, respectively [1]. Other MICS implantable antennas applying similar miniaturization techniques include a 3457- mm^3 PIFA with a serpentine radiator built on MACOR substrate ($\epsilon_r = 6.1$) [8], and a 6480- mm^3 antenna with a waffle-type radiator built on silicon substrate ($\epsilon_r = 3.1$) [9], both intended for generic body implantation (2/3 human muscle properties used to represent average body properties). Multilayer structures including vertically stacked radiating patches increase the length of the current flow and further assist in miniaturization. Reported skin-implantable stacked PIFAs occupy miniaturized volumes of 598 [10], 383 [11], 337 [12], and 32.7 mm^3 [5], [13]. Biocompatibility issues entail the use of a superstrate for all structures, while gain degradation with size reduction must also be considered.

Numerical models of implantable patch antennas proposed in the literature are generally simplified; zero-thickness perfectly conducting sheet model for the radiating and ground planes, glue used to bond the layers together is not taken into account, while ideal models of 50- Ω coaxial cables are used to feed the structures. Most studies report reflection coefficient measurements (e.g., [1], [2], [8]–[11]) without assessing the effect of fabrication/testing details on the resonance of the simplified antenna or discussing design refinements required to restore the desired performance. Only influence of the feeding network has been discussed for patch implantable antennas [14]; however, no design modifications were suggested to overcome its effects in antenna resonance. Preliminary investigations on metallization, gluing, and feeding considerations in numerical design have recently been reported for 3-D cylindrical antennas [15]. As the antenna dimensions shrink, the effect of fabrication issues becomes even more critical.

In this paper, the first challenge lies in proposing a novel design-and-testing methodology that optimizes the design of simplified implantable antennas to suit-specific prototype fabrication approaches. Antenna design is optimized based on quasi-Newton optimization [16] to address metallization, gluing, and feeding considerations, while sensitivity tests are performed to determine the maximum allowable deviations between numerical and experimental results. A low-cost technique is further suggested for reliably measuring the electric properties of (tissue-simulating) liquids without the use of commercial equipment.

The second challenge lies in dealing with prototype fabrication of miniature antennas for which tolerance to fabrication issues (e.g., soldering bumps, uncertainties in glue thickness and permittivity, etc.) is considered to be highly critical. A parametric model of a novel miniature antenna is proposed for skin implantation, and the design-and-testing methodology is applied to optimally adjust it within a specific fabrication/testing approach, for validation purposes. To speed up design while providing an antenna model for generic skin implantation (e.g., inside the head, arm, and trunk for intracranial pressure, blood pressure, and glucose monitoring, respectively [17]), investigations are performed inside a canonical skin-tissue model. Antenna performance is finally evaluated inside an anatomical head model (e.g., pressure monitoring, brain wave sensing, stroke rehabilitation, etc.).

An attempt is, thus, made to gain valuable insight into prototype fabrication and testing considerations that need to be considered within simulations for miniature implantable patch antennas. Although skin implantation in the MICS band is emphasized, the proposed methodology can easily be applied to optimize antennas for several other implantation scenarios and operation frequencies [18], [19]. This paper is organized as follows. Section II describes the proposed methods and models. Validation is performed in Section III. Numerical results inside an anatomical head model are presented in Section IV. This paper concludes in Section V.

II. MODELS AND METHODS

A. Tissue Models and Numerical Methods

To speed up simulations while providing a generic skin-implantable antenna, design and testing are performed inside a canonical skin-tissue model [see Fig. 1(a)] [5], [17]. The dimensions are those of a typical semifilled plastic drinking glass, while the antenna is considered to be immersed by 2 cm. Antenna resonance has been found to be almost insensitive to the shape of the tissue model, as long as it is surrounded by skin-tissue. Finite element (FE) simulations are carried out using the commercial software Ansoft HFSS [20]. The FE solver performs iterative tetrahedron-meshing refinement automatically with the mesh being perturbed by 30% between each pass. The mesh refinement procedure stops when the maximum change in the reflection coefficient magnitude ($|S_{11}|$) between two consecutive passes is less than 0.02 or when the number of passes exceeds 10.

Performance of the antenna is further examined inside a 13-tissue (see Table I) anatomical head model [see Fig. 1(b)] [5].

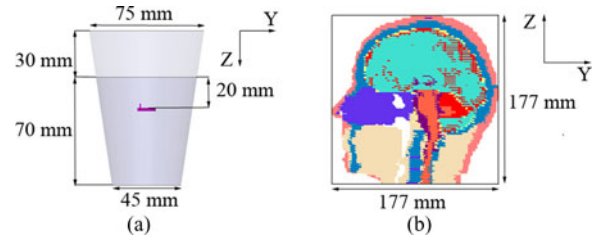


Fig. 1. Tissue models: (a) typical semi-filled plastic drinking glass and (b) 13-tissue anatomical human head.

TABLE I
TISSUE ELECTRIC PROPERTIES AT 402 MHz AND MASS DENSITIES

Biological Tissue	Permittivity (ϵ_r)	Conductivity (σ [S/m])	Mass Density (ρ [kg/m ³])
skin (dry)	46.74	0.69	1100
bone (cortical)	13.10	0.09	2200
dura	46.65	0.83	1100
cerebrospinal fluid	70.97	2.25	1020
grey matter	57.40	0.74	1030
white matter	42.05	0.45	1030
muscle	57.11	0.80	1040
cartilage	45.45	0.59	1100
vitreous humor	69.00	1.53	1000
lens	48.14	0.67	1100
eye sclera	57.66	1.00	1100
spinal cord	35.39	0.45	1040
cerebellum	55.94	1.03	1030

The antenna is implanted 3.6 mm under the skin, with its ground plane being placed in parallel with the horizontal plane of the head model. Finite-difference time-domain (FDTD) simulations are carried out in Remcom XFDTD [21], which enables efficient modeling of anatomical body parts. The antenna and anatomical head are modeled in 0.1- and 3.66-mm³ cells. Cells of 5 mm in edge Δx model free space to meet the FDTD spatial step constraint ($\Delta x < \lambda_{\min}/10$) where λ_{\min} indicates the wavelength of the highest frequency of interest) for the simulation set up under consideration. This sets the maximum simulation frequency f_{\max} to 6 GHz ($f_{\max} < c/(10\Delta x)$, where c is the speed of light), and the time step Δt to 9.622 ps ($\Delta t = \Delta x/c\sqrt{3}$), as referenced to free space. Meshing is adaptive to avoid abrupt transitions. A sinusoidal and a Gaussian source (pulse width of 32 time steps) are used in the single-frequency and broadband simulations. Calculations continue up to a 30-dB convergence.

Absorbing boundaries are set $\lambda_0/4$ (λ_0 is the free-space wavelength, $f_0 = 402$ MHz) away from all simulation setups in order to extend radiation infinitely far, while guaranteeing stability of the numerical calculations [20], [21]. Tissue electric properties at 402 MHz are considered (see Table I [22]), and approximated as constant inside the 300–500-MHz frequency range [5]. Tissue mass densities are also provided in Table I.

B. Parametric Antenna Model

A parametric model of a miniature stacked PIFA is proposed for skin implantation, as shown in Fig. 2.

Corresponding dimensions are indicated in Table II for a simplified antenna (simplified), an optimized antenna considering

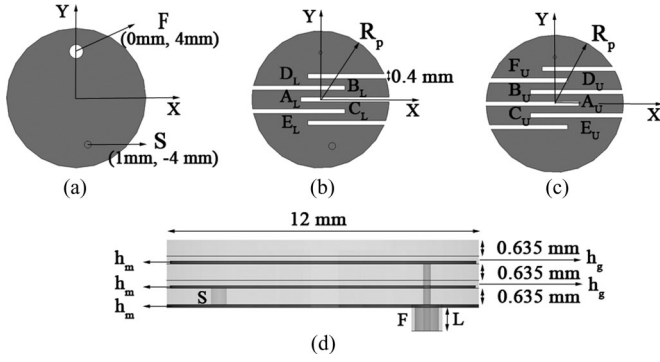


Fig. 2. Proposed parametric antenna model: (a) ground plane, (b) lower patch, (c) upper patch, and (d) side view.

TABLE II
VARIABLE VALUES OF THE PROPOSED SIMPLIFIED AND FABRICATION-SPECIFIC ANTENNAS (IN mm)

	simplified	fabrication-specific	head-tuned
h_m	0	0.017	0
ϵ_{rg}	–	2	–
h_g	0	0.3	0
coax type	simplified	EZ-47	simplified
L	1	50	1
R_p	5	5.9	5
x_{Al}	-1.3	-1.7	-2.0
x_{Bl}	3.8	4.3	3.8
x_{Cl}	3.8	4.3	3.8
x_{Dl}	2.5	2.6	2.5
x_{El}	2.5	2.6	2.5
x_{Au}	4.1	5.5	4.1
x_{Bu}	-3.8	-5.3	-3.8
x_{Cu}	-3.8	-5.3	-3.8
x_{Du}	2.5	4.9	3.4
x_{Eu}	2.5	4.9	3.4
x_{Fu}	-2.4	-3.8	-2.4

specific fabrication issues (fabrication-specific), and a fine-tuned version of the simplified antenna inside the anatomical head model of Fig. 1(b) (head-tuned). Circular shape is chosen to avoid sharp edges, while the origin of the coordinate system is considered to be located at the center of the PIFA ground plane. The model consists of a 6-mm radius ground plane and two R_p -radius vertically stacked, meandered patches. Copper sheets with a thickness of h_m are considered for the ground, lower, and upper patches. Both patches are fed by an L -length, 50- Ω coaxial cable (F: $x = 0$ mm, $y = 4$ mm), and radiate. Each one is printed on a 0.635-mm substrate (lower/upper), while a 0.635-mm superstrate covers the structure to preserve its biocompatibility and robustness. Rogers RO 3210 ($\epsilon_r = 10.2$, $\tan\delta = 0.003$), which has long been used in implantable antennas [1], [2], [10]–[12] is chosen as the dielectric material. Glue layers ($\epsilon_r = \epsilon_{rg}$) with a thickness of h_g bond the dielectric layers together. Meanders are equidistant by 1 mm, and their lengths are denoted by the x coordinate x_{ij} , where the subscripts $\{ij: i = A-F, \text{ and } j = L, U\}$ identify the meander in Fig. 2(b) and (c). Their width is designed to be small (0.4 mm) as to maximize the area of the patch for radiation. A 0.3-mm radius shorting pin (S: $x = 1$ mm,

TABLE III
EFFECT OF METALLIZATION, GLUING, AND FEEDING ON THE RESONANCE OF THE PROPOSED SIMPLIFIED ANTENNA

h_m [mm]	ϵ_{rg}	h_g [mm]	coax type	L [mm]	f_{res} [MHz]	$ S_{11@fres} $ [dB]
0	–	0	simplified	1	402	-46.9
17	–	0	simplified	1	403.5	-24.7
35	–	0	simplified	1	406.0	-23.4
70	–	0	simplified	1	409.0	-19.7
0	3	0.05	simplified	1	439.2	-17.3
0	3	0.1	simplified	1	460.3	-10.6
0	3	0.2	simplified	1	507.3	-6.9
0	2	0.05	simplified	1	446.2	-11.8
0	2	0.1	simplified	1	486.2	-7.8
0	2	0.2	simplified	1	546.4	-4.7
0	–	0	EZ-47	1	405.3	-39.8
0	–	0	EZ-47	10	401.2	-36.9
0	–	0	EZ-47	30	398.0	-28.4
0	–	0	EZ-47	60	398.0	-32.4

$y = -4$ mm) connects the ground plane with the lower patch for further miniaturization.

The simplified version of the parametric antenna model exhibits zero thickness, perfect electric ground- and patch-planes, ignoring the presence of glue, and is fed by a simplified $L = 1$ mm, 50- Ω coaxial cable (inner and outer conductors modeled as a perfect conductor cylinder and a zero-thickness perfect conducting sheet, respectively). Variable values shown in Table II under “simplified” are found to achieve a reflection coefficient magnitude ($|S_{11}|$) of being less than -25 dB in the MICS band. The effects of metallization (h_m), gluing (ϵ_{rg} , h_g), and feeding (coax type, L) are shown in Table III. Resonance characteristics are recorded, i.e., the exhibited resonance frequency f_{res} and $|S_{11@fres}|$. Gluing is found to be the most critical factor; low-permittivity glue layers isolate the high-permittivity substrate layers, thus decreasing the effective dielectric constant and electrical length of the antenna, while increasing its resonance frequency.

In a realistic prototype fabrication scenario, the metallization (h_m), gluing (ϵ_{rg} , h_g), and feeding (coax type, L) variables are set by the fabrication approach under consideration. Tuning the R_p and x_{ij} variables alters the effective dimensions of the antenna and helps achieve the desired resonance characteristics [23].

C. Design-and-Testing Methodology

An iterative design-and-testing methodology is proposed for implantable antennas, as summarized in Fig. 3. The basic idea is to optimize numerical antenna design for a specific prototype fabrication procedure and *in vitro* testing setup.

The simplified version of the parametric antenna model is initially optimized to address fabrication limitations and obtain the fabrication-specific antenna. Metallization (h_m), gluing (ϵ_{rg} , h_g), and feeding (coax type, L) variables are set to the values specified by the fabrication approach under consideration. The rest of the variables (R_p , x_{ij}) are considered as dimensions in the solution space and are optimized based on quasi-Newton optimization [16]. These are initialized to the values of the simplified antenna and vary within the range [5 mm, 5.9 mm] (R_p) and $[-(R_p - 0.3$ mm), $(R_p - 0.3$ mm)] (x_{ij}). The minimum and maximum step values are set to 0.1 and 0.4 mm, respectively. The cost function is defined as the magnitude of the

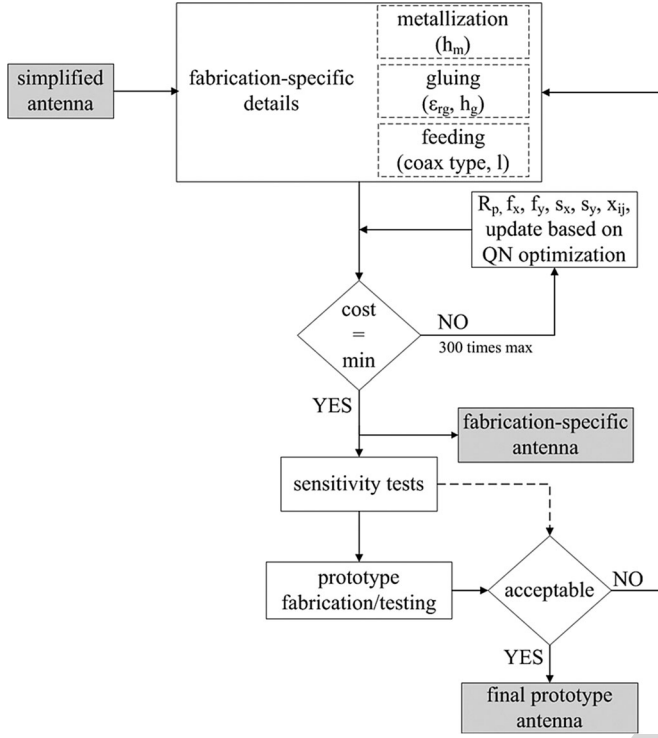


Fig. 3. Proposed design-and-testing methodology for implantable antennas.

coefficient at the desired resonance frequency of 402 MHz

$$\text{cost} = |S_{11@402\text{ MHz}}|. \quad (1)$$

Since the goal is to improve antenna resonance around 402 MHz, without aimlessly delaying design, the optimization process terminates when (1) is minimized, or when the number of iterations exceeds 300.

Numerical sensitivity tests are subsequently performed in order to assess what may be introduced within the *in vitro* testing of the fabrication-specific antenna. The effect of minor modifications in the most sensitive antenna design and testing parameters is examined, as imposed by the fabrication approach and measurement setup under consideration. Once the prototype antenna is fabricated and tested, sensitivity tests determine the maximum allowable deviation between numerical and experimental results, and the potential need for further refinement in numerical antenna design. Deviations within the acceptable limits mean that the final prototype antenna has been obtained.

D. Measurement of the Electric Properties of Liquids

In vitro testing of implantable antennas inside tissue-simulating liquids requires experimental measurement of the exhibited electric properties (ϵ_r , σ) to ensure conformance with the numerical values [22]. There exist commercial complex permittivity measurement systems (e.g., Agilent Technologies 85071E); however, alternative approaches are solicited for laboratories that are not equipped with such systems. A novel low-cost and reliable complex permittivity measurement technique is hereafter described and evaluated. To enhance confidence in measurements, the technique is both reflection-

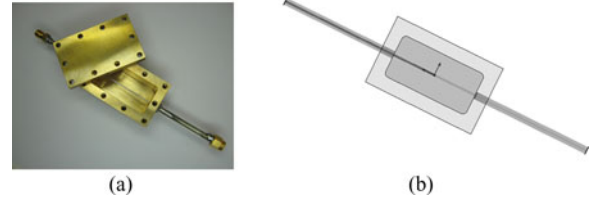


Fig. 4. (a) Coaxial container for complex permittivity measurement of liquid materials and (b) numerical model.

transmission-based rather than solely reflection-based, as is the usually reported case (e.g., [24] and [25]).

The measurement setup consists of a parallelepiped container intercepted by the inner conductor of a coaxial cable, as shown in Fig. 4(a). The arrangement corresponds to a coaxial container that can be filled with any liquid dielectric material. Its dimensions (exterior container of 52 mm × 32 mm × 32.2 mm, interior cavity of 40 mm × 20 mm × 20 mm) have been chosen so as to place a resonance mode around the desired measuring bandwidth of 300–500 MHz when filled with a high-permittivity liquid. After closing the container lid, the structure represents a transition between coaxial guides with a step characteristic impedance discontinuity. The transfer function between the two coaxial connectors outside the container depends upon the complex permittivity of the container's filling liquid. This can be de-embedded by comparing the measured scattering-matrix (S -matrix) with FE simulation results for the same structure. The simulation model is shown in Fig. 4(b), and is fine-tuned through experimental measurements for the empty (closed) container. In the case of nonhomogeneous mixtures, the present approach provides inherently an average permittivity value. The liquid is assumed to fill the inner volume of the container completely.

To validate the proposed experimental technique, measurements are carried out considering the container to be filled with a liquid with well-known properties, i.e., distilled water. In the simulations, the complex relative permittivity of distilled water is approximated by the Debye model as a function of frequency

$$\epsilon = \epsilon'_r - j\epsilon''_r = \epsilon_\infty + \frac{\epsilon_s - \epsilon_\infty}{1 + j\omega\tau} \quad (2)$$

where $\epsilon_\infty = 4.6$ is the optical permittivity at high frequencies, $\epsilon_s = 78.3$ is the static permittivity at low frequencies, and $\tau = 8.07$ ps is the electrical relaxation time [25]. Numerical and experimental results are superimposed in Fig. 5 indicating quite good agreement.

III. VALIDATION

Validation of the proposed design-and-testing methodology is performed within the framework of a specific fabrication process, as dictated by the available materials, assembling tools, and technical expertise/experience.

A. Prototype Fabrication Approach

Standard 0.017-mm electrodeposited copper foil covers both sides of Rogers RO 3210. The sheets are etched using a photolithographic process. The lower substrate layer contains

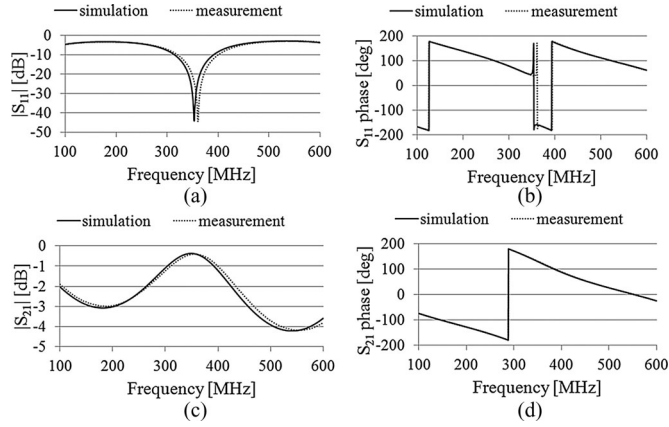


Fig. 5. Results for the coaxial container filled with distilled water: (a) magnitude of S_{11} ($|S_{11}|$), (b) phase of S_{11} (wrapped), (c) magnitude of S_{21} ($|S_{21}|$), and (d) phase of S_{21} (wrapped).

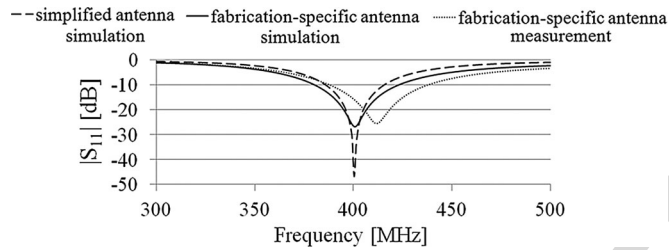


Fig. 6. Simulated and measured reflection coefficient frequency response of the simplified and fabrication-specific antennas.

294 the ground plane and the lower patch, the upper substrate contains
 295 the upper patch, and the superstrate has no metallization.
 296 Sprayable glue 3M 77 is used to bond the three layers ($\epsilon_r = 2$),
 297 which is found to exhibit an average thickness of 0.3 mm for
 298 the specific fabrication process. The antenna is fed through a
 299 50-mm long EZ-47 semi-rigid coaxial cable.

300 B. Validation

301 1) *Fabrication-Specific Antenna*: Metallization (h_m), gluing
 302 (ϵ_{rg} , h_g), and feeding (coaxial type, L) variables are set
 303 to the values imposed by the available fabrication approach,
 304 while the R_p and x_{ij} variables are optimized accordingly. Param-
 305 eter values shown in Table II under “fabrication-specific”
 306 are found to tune the fabrication-specific antenna at 402 MHz
 307 with a wide 10-dB bandwidth (defined at $|S_{11}| < -10$ dB)
 308 of 44 MHz covering the MICS band. Radii of the patches and
 309 meander lengths are significantly increased as compared to the
 310 simplified antenna. The aim is to counteract the increase in res-
 311 onance frequency imposed by the low-permittivity glue layers.
 312 The simulated reflection coefficient frequency responses of the
 313 simplified and fabrication-specific antennas are shown in Fig. 6.

314 2) *Sensitivity Tests*: Sensitivity test results related to antenna
 315 design and experimental phantom uncertainties are indicated in
 316 Figs. 7 and 8, respectively. Only the antenna or phantom param-
 317 eter under investigation is considered variable in each case, while
 318 all other parameters are kept constant and equal to those of the
 319 fabrication-specific antenna design (see Table II, fabrication-
 320 specific) and of the theoretical tissue model [see Fig. 1(a)].

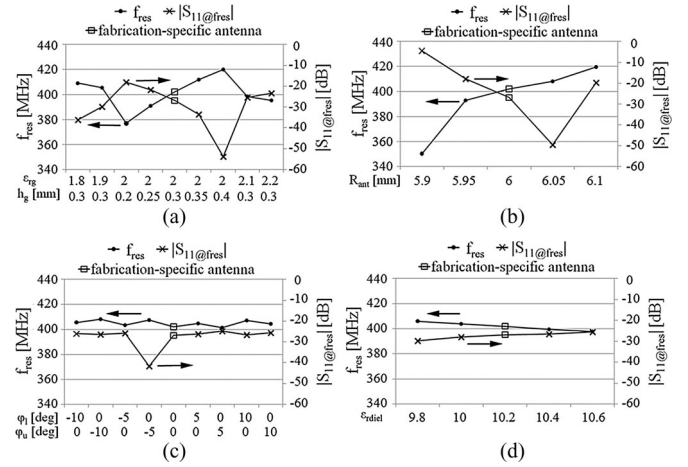


Fig. 7. Sensitivity test results (f_{res} , $|S_{11}@f_{res}|$) related to prototype antenna parameters: (a) gluing (ϵ_{rg} , h_g), (b) antenna radius R_{ant} , (c) rotation of the lower φ_l and upper φ_u patches, and (d) permittivity of the Rogers 3210 dielectric material, $\epsilon_{r,die}$.

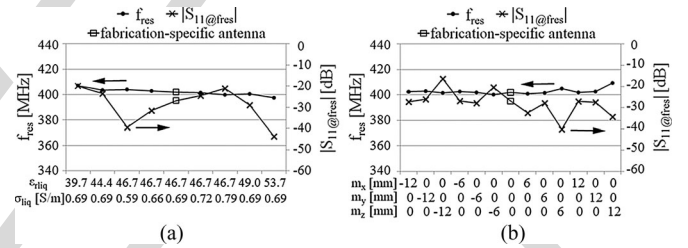


Fig. 8. Sensitivity test results (f_{res} , $|S_{11}@f_{res}|$) related to phantom parameters: (a) permittivity $\epsilon_{r,liq}$ and conductivity σ_{liq} of the skin-emulating liquid and (b) relative shift of the phantom from its original position (m_x , m_y , m_z).

Resonance characteristics including the resonance frequency f_{res} and $|S_{11}@f_{res}|$ are recorded, while the performance of the fabrication-specific antenna is also shown for reference. Given the fabrication approach described in Section III-A, the following parameters are identified as potential sources of experimental uncertainties, and examined.

- 1) *Gluing* (ϵ_{rg} , h_g) [see Fig. 7(a)]. Air bubbles accumulating within the glue prevent from being accurately determined. Furthermore, the adopted layer bonding process does not allow fine control of h_g . This is impaired not only by the glue itself, but also by the slight bump of the micro solder near the coaxial cable and the shorting pin that prevents perfect contact between the layers. Deviations of $\pm 10\%$ and 33% in ϵ_{rg} and h_g are found to cause frequency detunings by up to 1.7% and 6.2%, respectively;
- 2) *Antenna radius* R_{ant} [see Fig. 7(b)]. Rogers 3210 requires significant mechanical stress (vertical pressure and torsion) for detaching the excess alignment material degrading accuracy of the cutting procedure. A 0.2-mm increase in R_{ant} detunes the antenna by 4.4%, whereas a 0.1-mm decrease brings the copper patch sheets in direct contact with the tissue, thus, significantly degrading antenna resonance;
- 3) *Relative rotation between the patches* (indicated by the rotation of the lower φ_l and upper φ_u patches around

the z -axis) [see Fig. 7(c)]. Even though alignment marks are included in the photolithography masks, the alignment setup is relatively relaxed with respect to angular misalignment of the layers. Misalignment by 10° is found to cause a maximum frequency detuning of only 1.2%, thus, proving to be of minor importance. This justifies our choice for a relatively flexible alignment approach, while indicating the potential of relaxing the complexity of the assembling setup in order to benefit the gluing process that has been shown to be very critical. Positive and negative rotation angles correspond to clockwise and counterclockwise rotation around the z -axis, respectively;

- 4) *Permittivity of the Rogers 3210 dielectric material*, $\epsilon_{r\text{diel}}$ [see Fig. 7(d)]. The typical value of the Rogers 3210 permittivity is defined to be 10.2 at 10 GHz under 23°C . Frequency and temperature variations may slightly affect $\epsilon_{r\text{diel}}$ and degrade antenna performance. However, sensitivity tests indicate minor effects in antenna resonance; variations of ± 0.4 in $\epsilon_{r\text{diel}}$ may lead to frequency detunings by up to only 1%;
- 5) *Permittivity $\epsilon_{r\text{liq}}$ and conductivity σ_{liq} of the skin-simulating liquid* [see Fig. 8(a)]. Time and room temperature may perturb the properties of the mixture from their nominal values. Changes in $\epsilon_{r\text{liq}}$ and σ_{liq} by 15% are found to degrade antenna resonance by up to 1.2% and 0.5%, respectively;
- 6) *Relative antenna-phantom position (indicated by the relative shift of the phantom (m_x, m_y, m_z) from its original location)* [see Fig. 8(b)]. Since the antenna is manually positioned inside the phantom, slight deviations from the immersion scenario of Fig. 1(b) may occur. However, numerical results indicate insensitivity to antenna positioning inside the phantom as long as it is surrounded by skin-tissue.

3) *In Vitro Testing*: A skin-tissue-simulating liquid at 402 MHz is prepared (56.18% sugar, 2.33% salt, and 41.48% distilled water [2]) and its electric properties are measured using the technique described in Section II-D. Numerical and measured results are shown in Fig. 9, indicating adequacy of the mixture for *in vitro* testing. Dispersive, frequency-dependent ϵ_r and σ values of the skin-simulating liquid are used in the simulations, as shown in Fig. 10 (solid line) [2]. The ϵ_r and σ values of actual skin-tissue are also shown for reference (dotted line) [22].

The prototype antenna is further built [see Fig. 11(a)], connected to a network analyzer, and immersed inside the liquid [see Fig. 11(b)]. The measured reflection coefficient frequency response is shown in Fig. 6 (dotted line). Good agreement exists between numerical and experimental results. A slight resonance shift of 10 MHz (2.5%) is observed, which lies within the uncertainty allowances imposed by the sensitivity tests. Nevertheless, both simulation and measurement have an $|S_{11}| < -10$ dB bandwidth which includes the MICS band.

IV. PERFORMANCE INSIDE AN ANATOMICAL HEAD MODEL

The proposed antenna model is finally evaluated within the scalp-implantation scenario of Fig. 1(b). The simplified antenna

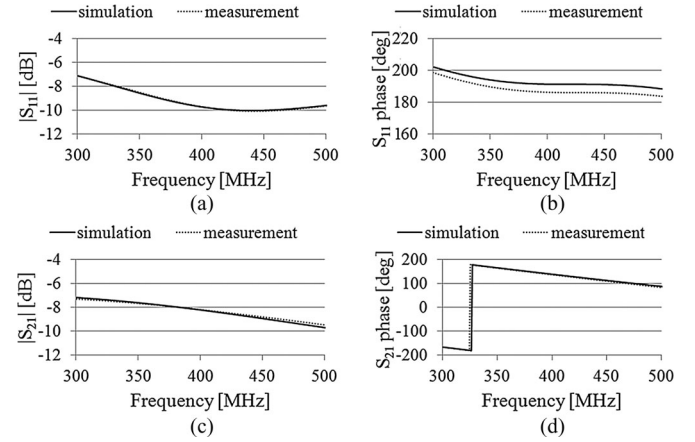


Fig. 9. Results for the coaxial container filled with skin-emulating liquid: (a) magnitude of S_{11} ($|S_{11}|$), (b) phase of S_{11} (wrapped), (c) magnitude of S_{21} ($|S_{21}|$), and (d) phase of S_{21} (wrapped).

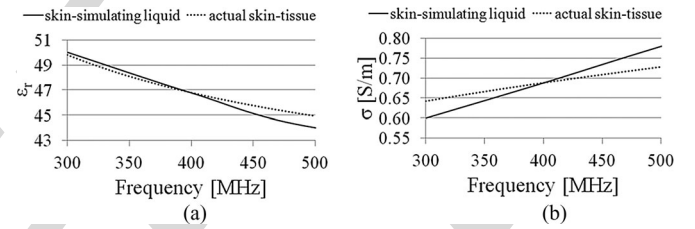


Fig. 10. Comparison of (a) permittivity ϵ_r and (b) conductivity σ of the skin-emulating liquid with the actual values for skin-tissue.

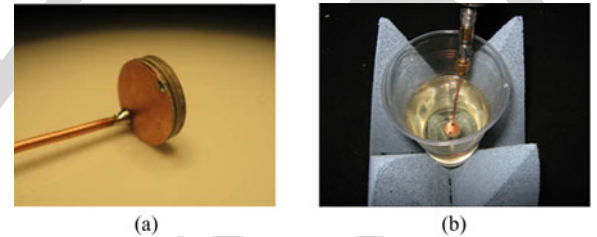


Fig. 11. (a) Fabricated prototype antenna and (b) *in vitro* testing setup.

is considered to provide generic results independent of the fabrication procedure, and fine-tuning is performed (see Table II under “head-tuned”) to achieve resonance in the MICS band [see Fig. 12(a)]. Detuning issues for implantable antennas inside specific anatomical locations have been discussed by the author [5], [17], and [26]. An infinitely thin wire and a $50\text{-}\Omega$ voltage source model the $50\text{-}\Omega$ coaxial feed exciting the antenna. The head-tuned antenna radiates an asymmetrical far-field gain radiation pattern [see Fig. 12(b)], with a maximum gain of -37.10 dBi exhibited in the $(\theta, \varphi) = (110^\circ, 90^\circ)$ direction. Low-gain values are attributed to the small PIFA size and high-tissue loss. Maximum 1-g-averaged (1-g-avg) and 10-g-averaged (10-g-avg) specific absorption rate (SAR) values equal 324.74 and 65.09 W/kg, respectively, for a net input power of 1 W. The IEEE C95.1-1999 (1-g-avg SAR ≤ 1.6 W/kg) and C95.1-2005 (10-g-avg SAR ≤ 2 W/kg) safety standards, thus, limit the maximum allowed net input power to 4.927 and 30.73 mW, respectively [27]. Local SAR distribution

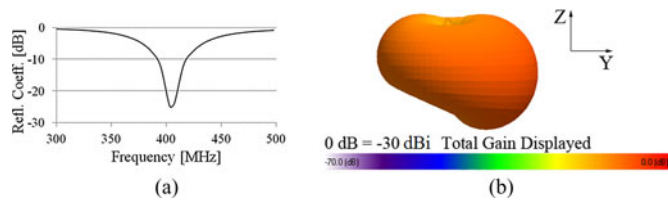


Fig. 12. (a) Reflection coefficient frequency response and (b) far-field gain radiation pattern of the head-tuned antenna implanted inside the anatomical head model [see Fig. 1(b)].

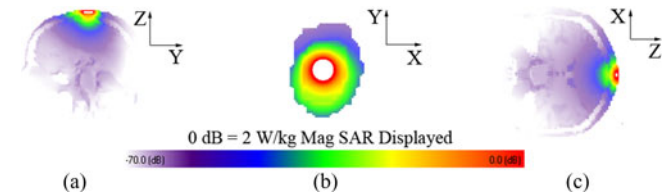


Fig. 13. Local SAR distribution in the (a) *yz*, (b) *xy*, and (c) *zx* slices of the anatomical head model [see Fig. 1(b)] where maximum local SAR values have been calculated (net input power = 4.927 mW).

considering a net-input power of 4.927 mW is shown in Fig. 13 for the slices where maximum local SAR values have been recorded.

V. CONCLUSION

We proposed a parametric model of a skin-implantable miniature PIFA for biotelemetry in the MICS band, and suggested a novel design-and-testing methodology for implantable antennas that incorporates gluing, metallization, and feeding considerations into numerical design. A low-cost, transmission-based technique was also described for reliably measuring the electric properties of liquids, without requiring specific commercial equipment.

Validation was further performed within a specific miniature-antenna-oriented fabrication approach. Sensitivity tests related to antenna design and phantom parameters indicated uncertainties of 0.5–6.2% in the exhibited resonance frequency, while relative antenna positioning was shown to be of minor significance. A resonance shift of 2.5% was observed in experimental testing as compared to simulations, which was within the expected uncertainty range.

Antenna implantation inside an anatomical head model required minor design modifications to refine tuning and exhibited an asymmetrical, low-gain (less than -37.10 dB) radiation pattern. Maximum net-input power levels of 4.927 and 30.73 mW were found to guarantee conformance with the IEEE C95.1-1999 and C95.1-2005 safety standards.

ACKNOWLEDGMENT

The authors would like to thank C. Brito and A. Almeida from Instituto Superior Técnico for prototype fabrication and measurement.

REFERENCES

- [1] J. Kim and Y. Rahmat-Samii, "Implanted antennas inside a human body: Simulations, designs and characterizations," *IEEE Trans. Microw. Theory Tech.*, vol. 52, no. 8, pp. 1934–1943, Aug. 2005.
- [2] T. Karacolak, A. Z. Hood, and E. Topsakal, "Design of a dual-band implantable antenna and development of skin mimicking gels for continuous glucose monitoring," *IEEE Trans. Microw. Theory Tech.*, vol. 56, no. 4, pp. 1001–1008, Apr. 2008.
- [3] R. Warty, M.-R. Tofighi, U. Kawoos, and A. Rosen, "Characterization of implantable antennas for intracranial pressure monitoring: Reflection by and transmission through a scalp phantom," *IEEE Trans. Microw. Theory Tech.*, vol. 56, no. 10, pp. 2366–2376, Oct. 2008.
- [4] L. Xu and M. Q.-H. Meng, "Effects of dielectric parameters of human body on radiation characteristics of ingestible wireless device at operating frequency of 430 MHz," *IEEE Trans. Biomed. Eng.*, vol. 56, no. 8, pp. 2083–2094, Aug. 2009.
- [5] A. Kiourti, M. Christopoulou, and K. S. Nikita, "Performance of a novel miniature antenna implanted in the human head for wireless biotelemetry," in *Proc. IEEE Int. Symp. Antennas Propag.*, Spokane, WA, 2011, pp. 392–395.
- [6] "Medical implant communications service (MICS) federal register," *Rules Reg.*, vol. 64, no. 240, pp. 69926–69934, Dec. 1999.
- [7] "European Radiocommunications Commission (ERC) Recommendation 70-03 relating to the use of short range devices," presented at the Conf. Eur. Postal. Telecomm. Admin. (EPT), 1997, Paper CEPT/ERC 70-03, Annex 12.
- [8] P. Soontornpipit, C. M. Furse, and Y. C. Chung, "Design of implantable microstrip antenna for communication with medical implants," *IEEE Trans. Microw. Theory Tech.*, vol. 52, no. 8, pp. 1944–1951, Aug. 2004.
- [9] P. Soontornpipit, C. M. Furse, and Y. C. Chung, "Miniaturized biocompatible microstrip antenna using genetic algorithm," *IEEE Trans. Antennas Propag.*, vol. 53, no. 6, pp. 1939–1945, Jun. 2005.
- [10] W.-C. Liu, F.-M. Yeh, and M. Ghavami, "Miniaturized implantable broadband antenna for biotelemetry communication," *Microw. Opt. Technol. Lett.*, vol. 50, pp. 2407–2409, Sep. 2008.
- [11] W.-C. Liu, S.-H. Chen, and C.-M. Wu, "Bandwidth enhancement and size reduction of an implantable PIFA antenna for biotelemetry devices," *Microw. Opt. Technol. Lett.*, vol. 51, pp. 755–757, Mar. 2009.
- [12] C.-M. Lee, T.-C. Yo, and C.-H. Luo, "Compact broadband stacked implantable antenna for biotelemetry with medical devices," in *Proc. IEEE Annu. Wireless Microw. Technol. Conf.*, Dec. 4–5, 2006, pp. 1–4.
- [13] A. Kiourti and K. S. Nikita, "Meandered versus spiral novel miniature PIFAs implanted in the human head: Tuning and performance," presented at the 2nd ICST Int. Conf. Wireless Mobile Commun. Healthcare, Kos Island, Greece, 2011, to be published.
- [14] F. Merli and A. K. Skrivervik, "Design and measurement considerations for implantable antennas for telemetry applications," in *Proc. 4th Europ. Conf. Antennas Propag.*, Barcelona, Spain, Apr. 2010, pp. 1–5.
- [15] F. Merli, L. Bolomey, J.-F. Zurcher, G. Corradini, E. Meurville, and A. K. Skrivervik, "Design, Realization and measurements of a miniature antenna for implantable wireless communication systems," *IEEE Trans. Antennas Propag.*, vol. 59, no. 10, pp. 3544–3555, Oct. 2011.
- [16] W. Sun and Y.-X. Yuan, *Optimization theory and methods*. New York: Springer-Verlag, 2006, ch. 5.
- [17] A. Kiourti and K. S. Nikita, "Detuning issues and performance of a novel implantable antenna for telemetry applications," presented at the 6th Europ. Conf. Antennas Propag., Prague, Czech Republic, Mar. 2012.
- [18] W. G. Scanlon and J. B. Burns, "Radiowave propagation from a tissue-implanted source at 418 MHz and 916.5 MHz," *IEEE Trans. Biomed. Eng.*, vol. 47, no. 4, pp. 527–534, Apr. 2000.
- [19] L. C. Chirwa, P. A. Hammond, S. Roy, and D. R. S. Cumming, "Electromagnetic radiation from ingested sources in the human intestine between 150 MHz and 1.2 GHz," *IEEE Trans. Biomed. Eng.*, vol. 50, no. 4, pp. 484–492, Apr. 2003.
- [20] *Ansoft High Frequency Structure Simulator (HFSS)*, Ver. 11, Ansoft Corporation, Pittsburgh, PA, 2008.
- [21] *XFDTD[®], Electromagnetic Solver Based on the Difference Time Domain Method*, Remcom, Inc., State College, PA, 2008.
- [22] C. Gabriel, S. Gabriel, and E. Corthout, "The dielectric properties of biological tissues," *Phys. Med. Biol.*, vol. 41, pp. 2231–2293, 1996.
- [23] A. Kiourti, M. Tsakalakis, and K. S. Nikita, "Parametric study and design of implantable PIFAs for wireless biotelemetry," presented at the Proc. 2nd ICST Int. Conf. Wireless Mobile Commun. Healthcare, Kos Island, Greece, 2011.

449

Q2

Q1

419
420
421
422





Q3

445
446
447
448

- 523 [24] D. Popovic, L. McCartney, C. Beasley, M. Lazebnik, M. Okoniewsky, 531
 524 S. C. Hagness, and J. H. Booske, "Precision open-ended coaxial probes 532
 525 for *in vivo* and *ex vivo* dielectric spectroscopy of biological tissues at 533
 526 microwave frequencies," *IEEE Trans. Microw. Theory Tech.*, vol. 53, 534
 527 no. 5, pp. 1713–1722, May 2005. [26] A. Kiourti and K. S. Nikita, "Miniature scalp-implantable antennas for 531
 528 [25] R. Zajicek, L. Oppl, and J. Vrbaf, "Broadband measurement of complex 532
 529 permittivity using reflection method and coaxial probes," *Radioengineer- 533
 530 ing*, vol. 17, pp. 14–19, Apr. 2008. [27] *IEEE Standard for Safety Levels with Respect to Human Exposure to 534
 535 Radiofrequency Electromagnetic Fields, 3 kHz to 300 GHz*, IEEE Standard 535
 C95.1-1999, 2005.
- Authors' photographs and biographies not available at the time of publication. 537
 538

IEEE
 Proof

QUERIES

- Q1. Author: Citation of “Fig.14” has been changed to “Fig. 13” in sentence “Local SAR . . . been recorded.” Please verify. 
- Q2. Author: Please provide name of the authors in Refs. [6], [7]. 
- Q3. Author: Please provide the year information in Refs. [13], [21]. 
- Q4. Author: Please update Ref. [26]. 

539

540

541

542

543

IEEE
Proof

Miniature Implantable Antennas for Biomedical Telemetry: From Simulation to Realization

Asimina Kiourti*, *Student Member, IEEE*, Jorge R. Costa, *Senior Member, IEEE*,
 Carlos A. Fernandes, *Senior Member, IEEE*, André G. Santiago, and Konstantina S. Nikita, *Senior Member, IEEE*

Abstract—We address numerical versus experimental design and testing of miniature implantable antennas for biomedical telemetry in the medical implant communications service band (402–405 MHz). A model of a novel miniature antenna is initially proposed for skin implantation, which includes varying parameters to deal with fabrication-specific details. An iterative design-and-testing methodology is further suggested to determine the parameter values that minimize deviations between numerical and experimental results. To assist *in vitro* testing, a low-cost technique is proposed for reliably measuring the electric properties of liquids without requiring commercial equipment. Validation is performed within a specific prototype fabrication/testing approach for miniature antennas. To speed up design while providing an antenna for generic skin implantation, investigations are performed inside a canonical skin-tissue model. Resonance, radiation, and safety performance of the proposed antenna is finally evaluated inside an anatomical head model. This study provides valuable insight into the design of implantable antennas, assessing the significance of fabrication-specific details in numerical simulations and uncertainties in experimental testing for miniature structures. The proposed methodology can be applied to optimize antennas for several fabrication/testing approaches and biotelemetry applications.

Index Terms—Biomedical telemetry, dielectric measurements, implantable antenna, *in vitro*, medical implant communications service (MICS) band.

I. INTRODUCTION

WIRELESS antenna telemetry for implantable biomedical devices is recently receiving considerable attention for diagnosis and therapy [1]–[5]. Bidirectional communication between the implanted device and exterior monitoring/control

Manuscript received February 14, 2012; revised April 5, 2012; accepted May 25, 2012. Date of publication; date of current version. This work was supported in part by the Fundação para a Ciência e Tecnologia, Portugal, under Project RFID Local PTDC/EEA-TEL/102390/2008. The work of A.K. was supported by the IEEE Antennas and Propagation Society Doctoral Research Award. Asterisk indicates corresponding author.

*A. Kiourti is with the School of Electrical and Computer Engineering and the Institute of Communications and Computer Systems, National Technical University of Athens, Athens 15780, Greece (e-mail: akiourti@biosim.ntua.gr).

J. R. Costa is with the Instituto de Telecomunicações and the Departamento de Ciências e Tecnologias da Informação, Instituto Universitário de Lisboa (ISCTE-IUL), Lisboa 1649-026, Portugal (e-mail: Jorge.Costa@lx.it.pt).

C. A. Fernandes is with Instituto de Telecomunicações and the Instituto Superior Técnico, Technical University of Lisbon, Lisboa 1049-001, Portugal (e-mail: carlos.fernandes@lx.it.pt).

A. G. Santiago is with Instituto Superior Técnico, Technical University of Lisbon, Lisboa 1049-001, Portugal (e-mail: andre.santiago.1988@gmail.com).

K. S. Nikita is with the School of Electrical and Computer Engineering and the Institute of Communications and Computer Systems, National Technical University of Athens, Athens 15780, Greece (e-mail: knikita@ece.ntua.gr).

Color versions of one or more of the figures in this paper are available online at <http://ieeexplore.ieee.org>.

Digital Object Identifier 10.1109/TBME.2012.2202659

equipment is most commonly performed in the medical implant communications service (MICS) band (402–405 MHz), which is regulated by the United States Federal Communications Commission [6] and the European Radiocommunications Committee [7]. Patch designs are preferred for implant-integrated antennas because of their flexibility in design, conformability, and shape [8].

Design of implantable patch antennas operating in the low-frequency MICS band draws high-scientific interest to deal with miniaturization. The aim is to decrease the antenna physical size, while increasing its electrical size. Rectangular 10 240- and 5760-mm³ chest-implantable antennas have been reported [1], which use the high-permittivity ($\epsilon_r = 10.2$) Rogers 3210 dielectric and apply a spiral radiator for size reduction. Addition of a shorting pin, thus, conversion to a planar inverted-F antenna (PIFA) acts like a ground plane on a monopole, and has been found to shrink the volume of the aforementioned antennas by 40% and 60%, respectively [1]. Other MICS implantable antennas applying similar miniaturization techniques include a 3457-mm³ PIFA with a serpentine radiator built on MACOR substrate ($\epsilon_r = 6.1$) [8], and a 6480-mm³ antenna with a waffle-type radiator built on silicon substrate ($\epsilon_r = 3.1$) [9], both intended for generic body implantation (2/3 human muscle properties used to represent average body properties). Multilayer structures including vertically stacked radiating patches increase the length of the current flow and further assist in miniaturization. Reported skin-implantable stacked PIFAs occupy miniaturized volumes of 598 [10], 383 [11], 337 [12], and 32.7 mm³ [5], [13]. Biocompatibility issues entail the use of a superstrate for all structures, while gain degradation with size reduction must also be considered.

Numerical models of implantable patch antennas proposed in the literature are generally simplified; zero-thickness perfectly conducting sheet model for the radiating and ground planes, glue used to bond the layers together is not taken into account, while ideal models of 50- Ω coaxial cables are used to feed the structures. Most studies report reflection coefficient measurements (e.g., [1], [2], [8]–[11]) without assessing the effect of fabrication/testing details on the resonance of the simplified antenna or discussing design refinements required to restore the desired performance. Only influence of the feeding network has been discussed for patch implantable antennas [14]; however, no design modifications were suggested to overcome its effects in antenna resonance. Preliminary investigations on metallization, gluing, and feeding considerations in numerical design have recently been reported for 3-D cylindrical antennas [15]. As the antenna dimensions shrink, the effect of fabrication issues becomes even more critical.

In this paper, the first challenge lies in proposing a novel design-and-testing methodology that optimizes the design of simplified implantable antennas to suit-specific prototype fabrication approaches. Antenna design is optimized based on quasi-Newton optimization [16] to address metallization, gluing, and feeding considerations, while sensitivity tests are performed to determine the maximum allowable deviations between numerical and experimental results. A low-cost technique is further suggested for reliably measuring the electric properties of (tissue-simulating) liquids without the use of commercial equipment.

The second challenge lies in dealing with prototype fabrication of miniature antennas for which tolerance to fabrication issues (e.g., soldering bumps, uncertainties in glue thickness and permittivity, etc.) is considered to be highly critical. A parametric model of a novel miniature antenna is proposed for skin implantation, and the design-and-testing methodology is applied to optimally adjust it within a specific fabrication/testing approach, for validation purposes. To speed up design while providing an antenna model for generic skin implantation (e.g., inside the head, arm, and trunk for intracranial pressure, blood pressure, and glucose monitoring, respectively [17]), investigations are performed inside a canonical skin-tissue model. Antenna performance is finally evaluated inside an anatomical head model (e.g., pressure monitoring, brain wave sensing, stroke rehabilitation, etc.).

An attempt is, thus, made to gain valuable insight into prototype fabrication and testing considerations that need to be considered within simulations for miniature implantable patch antennas. Although skin implantation in the MICS band is emphasized, the proposed methodology can easily be applied to optimize antennas for several other implantation scenarios and operation frequencies [18], [19]. This paper is organized as follows. Section II describes the proposed methods and models. Validation is performed in Section III. Numerical results inside an anatomical head model are presented in Section IV. This paper concludes in Section V.

II. MODELS AND METHODS

A. Tissue Models and Numerical Methods

To speed up simulations while providing a generic skin-implantable antenna, design, and testing are performed inside a canonical skin-tissue model [see Fig. 1(a)] [5], [17]. The dimensions are those of a typical semifilled plastic drinking glass, while the antenna is considered to be immersed by 2 cm. Antenna resonance has been found to be almost insensitive to the shape of the tissue model, as long as it is surrounded by skin-tissue. Finite element (FE) simulations are carried out using the commercial software Ansoft HFSS [20]. The FE solver performs iterative tetrahedron-meshing refinement automatically with the mesh being perturbed by 30% between each pass. The mesh refinement procedure stops when the maximum change in the reflection coefficient magnitude ($|S_{11}|$) between two consecutive passes is less than 0.02 or when the number of passes exceeds 10.

Performance of the antenna is further examined inside a 13-tissue (see Table I) anatomical head model [see Fig. 1(b)] [5].

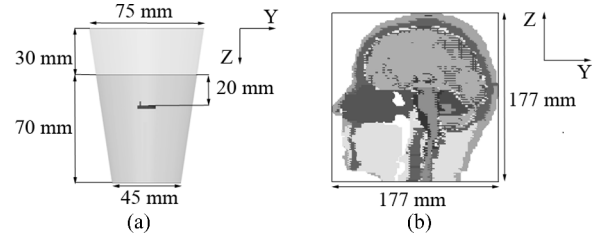


Fig. 1. Tissue models: (a) typical semi-filled plastic drinking glass and (b) 13-tissue anatomical human head.

TABLE I
TISSUE ELECTRIC PROPERTIES AT 402 MHz AND MASS DENSITIES

Biological Tissue	Permittivity (ϵ_r)	Conductivity (σ [S/m])	Mass Density (ρ [kg/m ³])
skin (dry)	46.74	0.69	1100
bone (cortical)	13.10	0.09	2200
dura	46.65	0.83	1100
cerebrospinal fluid	70.97	2.25	1020
grey matter	57.40	0.74	1030
white matter	42.05	0.45	1030
muscle	57.11	0.80	1040
cartilage	45.45	0.59	1100
vitreous humor	69.00	1.53	1000
lens	48.14	0.67	1100
eye sclera	57.66	1.00	1100
spinal cord	35.39	0.45	1040
cerebellum	55.94	1.03	1030

The antenna is implanted 3.6 mm under the skin, with its ground plane being placed in parallel with the horizontal plane of the head model. Finite-difference time-domain (FDTD) simulations are carried out in Remcom XFDTD [21], which enables efficient modeling of anatomical body parts. The antenna and anatomical head are modeled in 0.1- and 3.66-mm³ cells. Cells of 5 mm in edge Δx model free space so as to meet the FDTD spatial step constraint ($\Delta x < \lambda_{\min}/10$), where λ_{\min} indicates the wavelength of the highest frequency of interest) for the simulation set up under consideration. This sets the maximum simulation frequency f_{\max} to 6 GHz ($f_{\max} < c/(10\Delta x)$, where c is the speed of light, and the time step Δt to 9.622 ps ($\Delta t = \Delta x/c\sqrt{3}$), as referenced to free space. Meshing is adaptive to avoid abrupt transitions. A sinusoidal and a Gaussian source (pulse width of 32 time steps) are used in the single-frequency and broadband simulations. Calculations continue up to a 30-dB convergence.

Absorbing boundaries are set $\lambda_0/4$ (λ_0 is the free-space wavelength, $f_0 = 402$ MHz) away from all simulation setups in order to extend radiation infinitely far, while guaranteeing stability of the numerical calculations [20], [21]. Tissue electric properties at 402 MHz are considered (see Table I [22]), and approximated as constant inside the 300–500-MHz frequency range [5]. Tissue mass densities are also provided in Table I.

B. Parametric Antenna Model

A parametric model of a miniature stacked PIFA is proposed for skin implantation, as shown in Fig. 2.

Corresponding dimensions are indicated in Table II for a simplified antenna (simplified), an optimized antenna considering

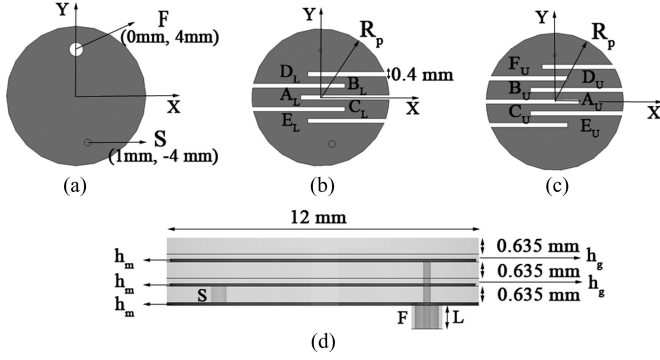


Fig. 2. Proposed parametric antenna model: (a) ground plane, (b) lower patch, (c) upper patch, and (d) side view.

TABLE II
VARIABLE VALUES OF THE PROPOSED SIMPLIFIED AND FABRICATION-SPECIFIC ANTENNAS (IN mm)

	simplified	fabrication-specific	head-tuned
h_m	0	0.017	0
ϵ_{rg}	–	2	–
h_g	0	0.3	0
coax type	simplified	EZ-47	simplified
L	1	50	1
R_p	5	5.9	5
x_{Al}	-1.3	-1.7	-2.0
x_{Bl}	3.8	4.3	3.8
x_{Cl}	3.8	4.3	3.8
x_{Dl}	2.5	2.6	2.5
x_{El}	2.5	2.6	2.5
x_{Au}	4.1	5.5	4.1
x_{Bu}	-3.8	-5.3	-3.8
x_{Cu}	-3.8	-5.3	-3.8
x_{Du}	2.5	4.9	3.4
x_{Eu}	2.5	4.9	3.4
x_{Fu}	-2.4	-3.8	-2.4

specific fabrication issues (fabrication specific), and a fine-tuned version of the simplified antenna inside the anatomical head model of Fig. 1(b) (head-tuned). Circular shape is chosen to avoid sharp edges, while the origin of the coordinate system is considered to be located at the center of the PIFA ground plane. The model consists of a 6-mm radius ground plane and two R_p -radius vertically stacked, meandered patches. Copper sheets with a thickness of h_m are considered for the ground, lower, and upper patches. Both patches are fed by an L -length, 50- Ω coaxial cable (F: $x = 0$ mm, $y = 4$ mm), and radiate. Each one is printed on a 0.635-mm substrate (lower/upper), while a 0.635-mm superstrate covers the structure to preserve its biocompatibility and robustness. Rogers RO 3210 ($\epsilon_r = 10.2$, $\tan\delta = 0.003$), which has long been used in implantable antennas [1], [2], [10]–[12] is chosen as the dielectric material. Glue layers ($\epsilon_r = \epsilon_{rg}$) with a thickness of h_g bond the dielectric layers together. Meanders are equidistant by 1 mm, and their lengths are denoted by the x coordinate x_{ij} , where the subscripts $\{ij: i = A-F, \text{ and } j = L, U\}$ identify the meander in Fig. 2(b) and (c). Their width is designed to be small (0.4 mm) so as to maximize the area of the patch for radiation. A 0.3-mm radius shorting pin (S: $x = 1$ mm,

TABLE III
EFFECT OF METALLIZATION, GLUING, AND FEEDING ON THE RESONANCE OF THE PROPOSED SIMPLIFIED ANTENNA

h_m [mm]	ϵ_{rg}	h_g [mm]	coax type	L [mm]	f_{res} [MHz]	$ S_{11@fres} $ [dB]
0	–	0	simplified	1	402	-46.9
17	–	0	simplified	1	403.5	-24.7
35	–	0	simplified	1	406.0	-23.4
70	–	0	simplified	1	409.0	-19.7
0	3	0.05	simplified	1	439.2	-17.3
0	3	0.1	simplified	1	460.3	-10.6
0	3	0.2	simplified	1	507.3	-6.9
0	2	0.05	simplified	1	446.2	-11.8
0	2	0.1	simplified	1	486.2	-7.8
0	2	0.2	simplified	1	546.4	-4.7
0	–	0	EZ-47	1	405.3	-39.8
0	–	0	EZ-47	10	401.2	-36.9
0	–	0	EZ-47	30	398.0	-28.4
0	–	0	EZ-47	60	398.0	-32.4

$y = -4$ mm) connects the ground plane with the lower patch for further miniaturization.

The simplified version of the parametric antenna model exhibits zero thickness, perfect electric ground- and patch-planes, ignores the presence of glue, and is fed by a simplified $L = 1$ mm, 50- Ω coaxial cable (inner and outer conductors modeled as a perfect conductor cylinder and a zero-thickness perfect conducting sheet, respectively). Variable values shown in Table II under “simplified” are found to achieve a reflection coefficient magnitude ($|S_{11}|$) of better than -25 dB in the MICS band. The effects of metallization h_m , gluing (ϵ_{rg} , h_g), and feeding (coax type, L) are shown in Table III. Resonance characteristics are recorded, i.e., the exhibited resonance frequency f_{res} and $|S_{11@fres}|$. Gluing is found to be the most critical factor; low-permittivity glue layers isolate the high-permittivity substrate layers, thus decreasing the effective dielectric constant and electrical length of the antenna, while increasing its resonance frequency.

In a realistic prototype fabrication scenario, the metallization h_m , gluing (ϵ_{rg} , h_g), and feeding (coax type, L) variables are set by the fabrication approach under consideration. Tuning the R_p and x_{ij} variables alters the effective dimensions of the antenna and helps achieve the desired resonance characteristics [23].

C. Design-and-Testing Methodology

An iterative design-and-testing methodology is proposed for implantable antennas, as summarized in Fig. 3. The basic idea is to optimize numerical antenna design for a specific prototype fabrication procedure and *in vitro* testing setup.

The simplified version of the parametric antenna model is initially optimized to address fabrication limitations and obtain the fabrication-specific antenna. Metallization (h_m), gluing (ϵ_{rg} , h_g), and feeding (coax type, L) variables are set to the values specified by the fabrication approach under consideration. The rest of the variables (R_p , x_{ij}) are considered as dimensions in the solution space and are optimized based on quasi-Newton optimization [16]. These are initialized to the values of the simplified antenna and vary within the range [5 mm, 5.9 mm] (R_p) and $[-(R_p - 0.3$ mm), $(R_p - 0.3$ mm)] (x_{ij}). The minimum and maximum step values are set to 0.1 and 0.4 mm, respectively. The cost function is defined as the magnitude of the reflection

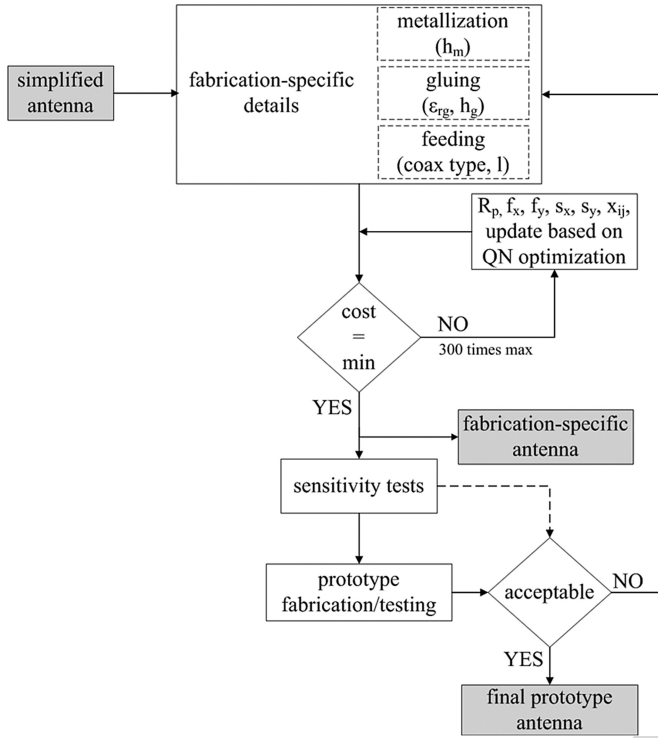


Fig. 3. Proposed design-and-testing methodology for implantable antennas.

coefficient at the desired resonance frequency of 402 MHz

$$\text{cost} = |S_{11@402\text{ MHz}}|. \quad (1)$$

Since the goal is to improve antenna resonance around 402 MHz, without aimlessly delaying design, the optimization process terminates when (1) is minimized, or when the number of iterations exceeds 300.

Numerical sensitivity tests are subsequently performed in order to assess that may be introduced within the *in vitro* testing of the fabrication-specific antenna. The effect of minor modifications in the most sensitive antenna design and testing parameters is examined, as imposed by the fabrication approach and measurement setup under consideration. Once the prototype antenna is fabricated and tested, sensitivity tests determine the maximum allowable deviation between numerical and experimental results, and the potential need for further refinement in numerical antenna design. Deviations within the acceptable limits mean that the final prototype antenna has been obtained.

D. Measurement of the Electric Properties of Liquids

In vitro testing of implantable antennas inside tissue-simulating liquids requires experimental measurement of the exhibited electric properties (ϵ_r , σ) to ensure conformance with the numerical values [22]. There exist commercial complex permittivity measurement systems (e.g., Agilent Technologies 85071E); however, alternative approaches are solicited for laboratories that are not equipped with such systems. A novel low-cost and reliable complex permittivity measurement technique is hereafter described and evaluated. To enhance confidence in measurements, the technique is both reflection- and

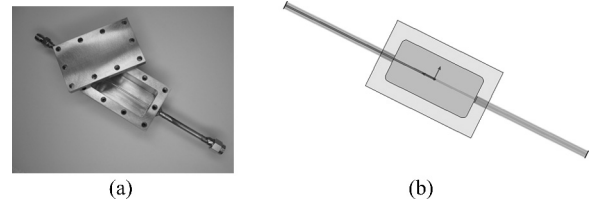


Fig. 4. (a) Coaxial container for complex permittivity measurement of liquid materials and (b) numerical model.

transmission-based rather than solely reflection-based, as is the usually reported case (e.g., [24] and [25]).

The measurement setup consists of a parallelepiped container intercepted by the inner conductor of a coaxial cable, as shown in Fig. 4(a). The arrangement corresponds to a coaxial container that can be filled with any liquid dielectric material. Its dimensions (exterior container of 52 mm × 32 mm × 32.2 mm, interior cavity of 40 mm × 20 mm × 20 mm) have been chosen so as to place a resonance mode around the desired measuring bandwidth of 300–500 MHz when filled with a high-permittivity liquid. After closing the container lid, the structure represents a transition between coaxial guides with a step characteristic impedance discontinuity. The transfer function between the two coaxial connectors outside the container depends upon the complex permittivity of the container's filling liquid. This can be de-embedded by comparing the measured scattering-matrix (S -matrix) with FE simulation results for the same structure. The simulation model is shown in Fig. 4(b), and is fine-tuned through experimental measurements for the empty (closed) container. In the case of nonhomogeneous mixtures, the present approach provides inherently an average permittivity value. The liquid is assumed to fill the inner volume of the container completely.

To validate the proposed experimental technique, measurements are carried out considering the container to be filled with a liquid with well-known properties, i.e., distilled water. In the simulations, the complex relative permittivity of distilled water is approximated by the Debye model as a function of frequency

$$\epsilon = \epsilon'_r - j\epsilon''_r = \epsilon_\infty + \frac{\epsilon_s - \epsilon_\infty}{1 + j\omega\tau} \quad (2)$$

where $\epsilon_\infty = 4.6$ is the optical permittivity at high frequencies, $\epsilon_s = 78.3$ is the static permittivity at low frequencies, and $\tau = 8.07$ ps is the electrical relaxation time [25]. Numerical and experimental results are superimposed in Fig. 5 indicating quite good agreement.

III. VALIDATION

Validation of the proposed design-and-testing methodology is performed within the framework of a specific fabrication process, as dictated by the available materials, assembling tools, and technical expertise/experience.

A. Prototype Fabrication Approach

Standard 0.017-mm-thick electrodeposited copper foil covers both sides of Rogers RO 3210. The sheets are etched using a photolithographic process. The lower substrate layer contains

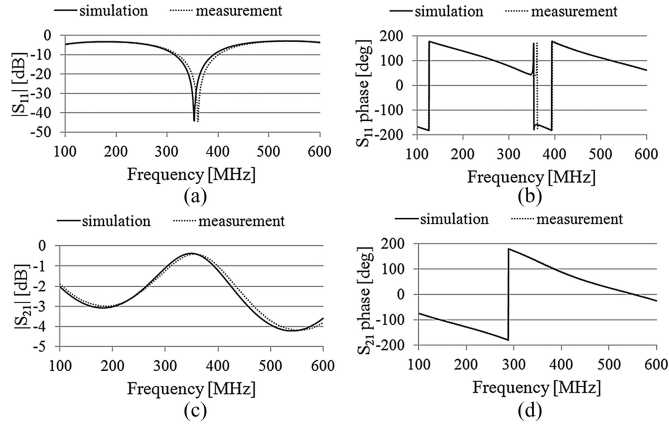


Fig. 5. Results for the coaxial container filled with distilled water: (a) magnitude of S_{11} ($|S_{11}|$), (b) phase of S_{11} (wrapped), (c) magnitude of S_{21} ($|S_{21}|$), and (d) phase of S_{21} (wrapped).

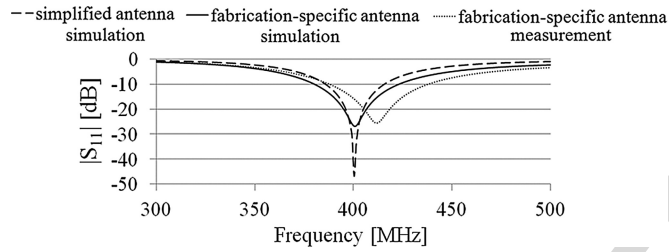


Fig. 6. Simulated and measured reflection coefficient frequency response of the simplified and fabrication-specific antennas.

294 the ground plane and the lower patch, the upper substrate contains
 295 the upper patch, and the superstrate has no metallization.
 296 Sprayable glue 3M 77 is used to bond the three layers ($\epsilon_r = 2$),
 297 which is found to exhibit an average thickness of 0.3 mm for
 298 the specific fabrication process. The antenna is fed through a
 299 50-mm long EZ-47 semirigid coaxial cable.

300 B. Validation

301 1) *Fabrication-Specific Antenna*: Metallization (h_m), gluing
 302 (ϵ_{rg} , h_g), and feeding (coaxial type, L) variables are set
 303 to the values imposed by the available fabrication approach,
 304 while the R_p and x_{ij} variables are optimized accordingly. Parameter
 305 values shown in Table II under “fabrication-specific”
 306 are found to tune the fabrication-specific antenna at 402 MHz
 307 with a wide 10-dB bandwidth (defined at $|S_{11}| < -10$ dB)
 308 of 44 MHz covering the MICS band. Radii of the patches and
 309 meander lengths are significantly increased as compared to the
 310 simplified antenna. The aim is to counteract the increase in resonance
 311 frequency imposed by the low-permittivity glue layers. The simulated
 312 reflection coefficient frequency responses of the simplified and fabrication-specific
 313 antennas are shown in Fig. 6.

314 2) *Sensitivity Tests*: Sensitivity test results related to antenna
 315 design and experimental phantom uncertainties are indicated in
 316 Figs. 7 and 8, respectively. Only the antenna or phantom parameter
 317 under investigation is considered variable in each case, while
 318 all other parameters are kept constant and equal to those of the
 319 fabrication-specific antenna design (see Table II, fabrication-specific)
 320 and of the theoretical tissue model [see Fig. 1(a)].

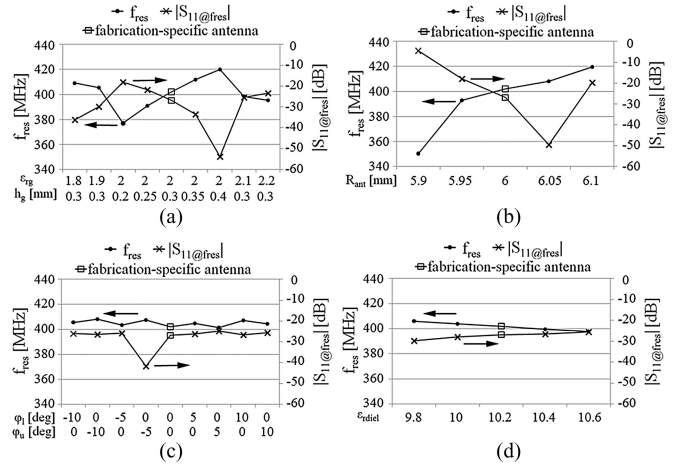


Fig. 7. Sensitivity test results (f_{res} , $|S_{11}@f_{res}|$) related to prototype antenna parameters: (a) gluing (ϵ_{rg} , h_g), (b) antenna radius R_{ant} , (c) rotation of the lower φ_l and upper φ_u patches, and (d) permittivity of the Rogers 3210 dielectric material, $\epsilon_{r\ diel}$.

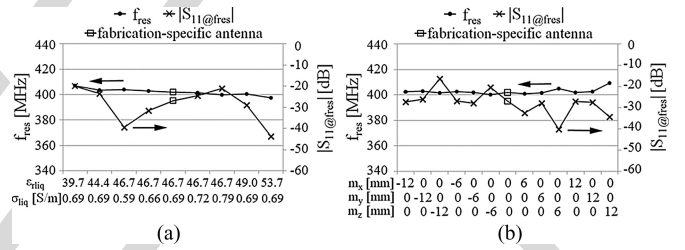


Fig. 8. Sensitivity test results (f_{res} , $|S_{11}@f_{res}|$) related to phantom parameters: (a) permittivity $\epsilon_{r\ liq}$ and conductivity σ_{liq} of the skin-emulating liquid and (b) relative shift of the phantom from its original position (m_x , m_y , m_z).

Resonance characteristics including the resonance frequency f_{res} and $|S_{11}@f_{res}|$ are recorded, while the performance of the fabrication-specific antenna is also shown for reference. Given the fabrication approach described in Section III-A, the following parameters are identified as potential sources of experimental uncertainties, and examined.

- 327 1) *Gluing* (ϵ_{rg} , h_g) [see Fig. 7(a)]. Air bubbles accumulating
 328 within the glue prevent f_{res} from being accurately determined. Furthermore,
 329 the adopted layer bonding process does not allow fine control of h_g . This is
 330 impaired not only by the glue itself, but also by the slight bump of the
 331 microsolder near the coaxial cable and the shorting pin that prevents perfect
 332 contact between the layers. Deviations of $\pm 10\%$ and 33% in ϵ_{rg} and h_g
 333 are found to cause frequency detunings by up to 1.7% and 6.2%, respectively;
 335
- 336 2) *Antenna radius* R_{ant} [see Fig. 7(b)]. Rogers 3210 requires significant
 337 mechanical stress (vertical pressure and torsion) for detaching the excess
 338 alignment material, thus degrading accuracy of the cutting procedure. A
 339 0.2-mm increase in R_{ant} detunes the antenna by 4.4%, whereas a 0.1-mm
 340 decrease brings the copper patch sheets in direct contact with the tissue,
 341 thus, significantly degrading antenna resonance;
 343
- 344 3) *Relative rotation between the patches* (indicated by the rotation
 345 of the lower φ_l and upper φ_u patches around

the z -axis) [see Fig. 7(c)]. Even though alignment marks are included in the photolithography masks, the alignment setup is relatively relaxed with respect to angular misalignment of the layers. Misalignment by 10° is found to cause a maximum frequency detuning of only 1.2%, thus, proving to be of minor importance. This justifies our choice for a relatively flexible alignment approach, while indicating the potential of relaxing the complexity of the assembling setup in order to benefit the gluing process that has been shown to be very critical. Positive and negative rotation angles correspond to clockwise and counterclockwise rotation around the z -axis, respectively;

- 4) *Permittivity of the Rogers 3210 dielectric material*, ϵ_{rdiel} [see Fig. 7(d)]. The typical value of the Rogers 3210 permittivity is defined to be 10.2 at 10 GHz under 23°C . Frequency and temperature variations may slightly affect ϵ_{rdiel} and degrade antenna performance. However, sensitivity tests indicate minor effects in antenna resonance, variations of ± 0.4 in ϵ_{rdiel} may lead to frequency detunings by up to only 1%;
- 5) *Permittivity ϵ_{rliq} and conductivity σ_{liq} of the skin-simulating liquid* [see Fig. 8(a)]. Time and room temperature may perturb the properties of the mixture from their nominal values. Changes in ϵ_{rliq} and σ_{liq} by 15% are found to degrade antenna resonance by up to 1.2% and 0.5%, respectively;
- 6) *Relative antenna-phantom position (indicated by the relative shift of the phantom (m_x, m_y, m_z) from its original location)* [see Fig. 8(b)]. Since the antenna is manually positioned inside the phantom, slight deviations from the immersion scenario of Fig. 1(b) may occur. However, numerical results indicate insensitivity to antenna positioning inside the phantom as long as it is surrounded by skin-tissue.

3) *In Vitro Testing*: A skin-tissue-simulating liquid at 402 MHz is prepared (56.18% sugar, 2.33% salt, and 41.48% distilled water [2]) and its electric properties are measured using the technique described in Section II-D. Numerical and measured results are shown in Fig. 9, indicating adequacy of the mixture for *in vitro* testing. Dispersive, frequency-dependent ϵ_r and σ values of the skin-simulating liquid are used in the simulations, as shown in Fig. 10 (solid line) [2]. The ϵ_r and σ values of actual skin-tissue are also shown for reference (dotted line) [22].

The prototype antenna is further built [see Fig. 11(a)], connected to a network analyzer, and immersed inside the liquid [see Fig. 11(b)]. The measured reflection coefficient frequency response is shown in Fig. 6 (dotted line). Good agreement exists between numerical and experimental results. A slight resonance shift of 10 MHz (2.5%) is observed, which lies within the uncertainty allowances imposed by the sensitivity tests. Nevertheless, both simulation and measurement have an $|S_{11}| < -10$ dB bandwidth which includes the MICS band.

IV. PERFORMANCE INSIDE AN ANATOMICAL HEAD MODEL

The proposed antenna model is finally evaluated within the scalp-implantation scenario of Fig. 1(b). The simplified antenna

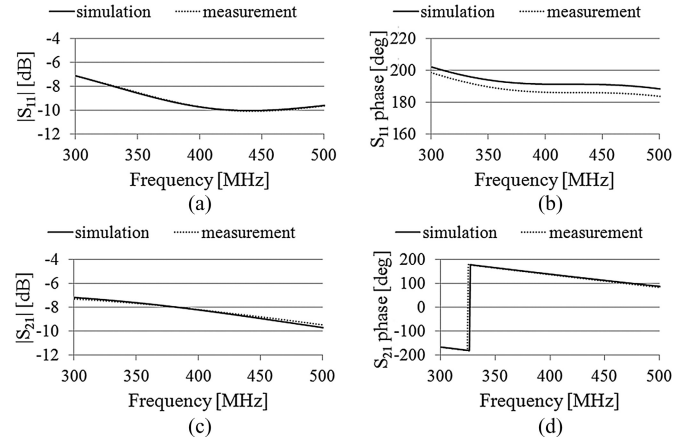


Fig. 9. Results for the coaxial container filled with skin-emulating liquid: (a) magnitude of S_{11} ($|S_{11}|$), (b) phase of S_{11} (wrapped), (c) magnitude of S_{21} ($|S_{21}|$), and (d) phase of S_{21} (wrapped).

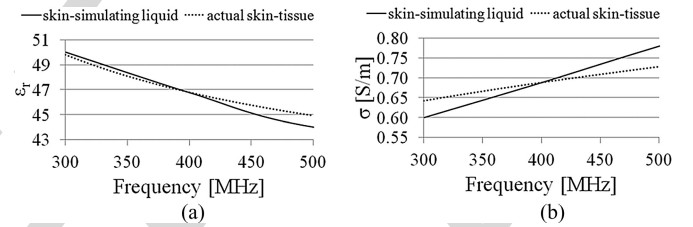


Fig. 10. Comparison of (a) permittivity ϵ_r and (b) conductivity σ of the skin-emulating liquid with the actual values for skin-tissue.

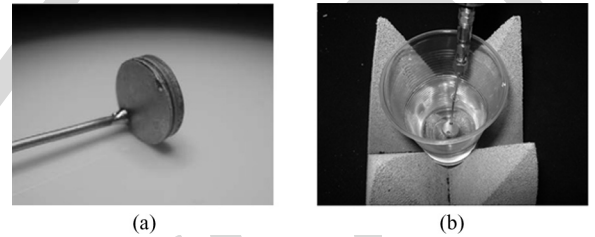


Fig. 11. (a) Fabricated prototype antenna and (b) *in vitro* testing setup.

is considered to provide generic results independent of the fabrication procedure, and fine-tuning is performed (see Table II under “head-tuned”) to achieve resonance in the MICS band [see Fig. 12(a)]. Detuning issues for implantable antennas inside specific anatomical locations have been discussed by the authors in [5], [17], and [26]. An infinitesimally thin wire and a $50\text{-}\Omega$ voltage source model the $50\text{-}\Omega$ coaxial feed exciting the antenna. The head-tuned antenna radiates an asymmetrical far-field gain radiation pattern [see Fig. 12(b)], with a maximum gain of -37.10 dBi exhibited in the $(\theta, \varphi) = (110^\circ, 90^\circ)$ direction. Low-gain values are attributed to the small PIFA size and high-tissue loss. Maximum 1-g-averaged (1-g-avg) and 10-g-averaged (10-g-avg) specific absorption rate (SAR) values equal 324.74 and 65.09 W/kg, respectively, for a net input power of 1 W. The IEEE C95.1-1999 (1-g-avg SAR ≤ 1.6 W/kg) and C95.1-2005 (10-g-avg SAR ≤ 2 W/kg) safety standards, thus, limit the maximum allowed net input power to 4.927 and 30.73 mW, respectively [27]. Local SAR distribution

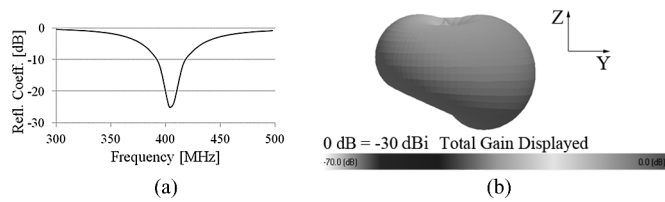


Fig. 12. (a) Reflection coefficient frequency response and (b) far-field gain radiation pattern of the head-tuned antenna implanted inside the anatomical head model [see Fig. 1(b)].

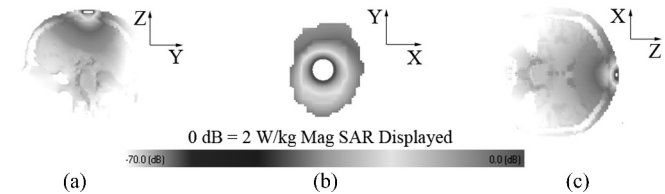


Fig. 13. Local SAR distribution in the (a) *yz*, (b) *xy*, and (c) *zx* slices of the anatomical head model [see Fig. 1(b)] where maximum local SAR values have been calculated (net input power = 4.927 mW).

419 considering a net-input power of 4.927 mW is shown in Fig. 13
 420 for the slices where maximum local SAR values have been
 Q1 421 recorded.

V. CONCLUSION

423 We proposed a parametric model of a skin-implantable minia-
 424 ture PIFA for biotelemetry in the MICS band, and suggested a
 425 novel design-and-testing methodology for implantable antennas
 426 that incorporates gluing, metallization, and feeding consider-
 427 ations into numerical design. A low-cost, transmission-based
 428 technique was also described for reliably measuring the elec-
 429 tric properties of liquids, without requiring specific commercial
 430 equipment.

431 Validation was further performed within a specific miniature-
 432 antenna-oriented fabrication approach. Sensitivity tests related
 433 to antenna design and phantom parameters indicated uncertain-
 434 ties of 0.5–6.2% in the exhibited resonance frequency, while
 435 relative antenna positioning was shown to be of minor signifi-
 436 cance. A resonance shift of 2.5% was observed in experimental
 437 testing as compared to simulations, which was within the ex-
 438 pected uncertainty range.

439 Antenna implantation inside an anatomical head model re-
 440 quired minor design modifications to refine tuning and exhib-
 441 ited an asymmetrical, low-gain (less than –37.10 dB) radiation pat-
 442 tern. Maximum net-input power levels of 4.927 and 30.73 mW
 443 were found to guarantee conformance with the IEEE C95.1-
 444 1999 and C95.1-2005 safety standards.

ACKNOWLEDGMENT

445 The authors would like to thank C. Brito and A. Almeida
 446 from Instituto Superior Técnico for prototype fabrication and
 447 measurement.
 448

REFERENCES

449
 450 [1] J. Kim and Y. Rahmat-Samii, “Implanted antennas inside a human body: 450
 451 Simulations, designs and characterizations,” *IEEE Trans. Microw. Theory*
 452 *Tech.*, vol. 52, no. 8, pp. 1934–1943, Aug. 2005.
 453 [2] T. Karacolak, A. Z. Hood, and E. Topsakal, “Design of a dual-band im- 453
 454 plantable antenna and development of skin mimicking gels for continuous
 455 glucose monitoring,” *IEEE Trans. Microw. Theory Tech.*, vol. 56, no. 4,
 456 pp. 1001–1008, Apr. 2008.
 457 [3] R. Warty, M.-R. Tofighi, U. Kawoos, and A. Rosen, “Characterization of 457
 458 implantable antennas for intracranial pressure monitoring: Reflection by
 459 and transmission through a scalp phantom,” *IEEE Trans. Microw. Theory*
 460 *Tech.*, vol. 56, no. 10, pp. 2366–2376, Oct. 2008.
 461 [4] L. Xu and M. Q.-H. Meng, “Effects of dielectric parameters of human 461
 462 body on radiation characteristics of ingestible wireless device at operat-
 463 ing frequency of 430 MHz,” *IEEE Trans. Biomed. Eng.*, vol. 56, no. 8,
 464 pp. 2083–2094, Aug. 2009.
 465 [5] A. Kiourti, M. Christopoulou, and K. S. Nikita, “Performance of a novel 465
 466 miniature antenna implanted in the human head for wireless biotelemetry,”
 467 in *Proc. IEEE Int. Symp. Antennas Propag.*, Spokane, WA, 2011, pp. 392–
 468 395.
 469 [6] “Medical implant communications service (MICS) federal register,” *Rules*
 470 *Reg.*, vol. 64, no. 240, pp. 69926–69934, Dec. 1999.
 471 [7] “European Radiocommunications Commission (ERC) Recommendation 471
 472 70-03 relating to the use of short range devices,” presented at the Conf.
 473 Eur. Postal. Telecomm. Admin. (EPT), 1997, Paper CEPT/ERC 70-03,
 474 Annex 12.
 475 [8] P. Soontornpipit, C. M. Furse, and Y. C. Chung, “Design of implantable 475
 476 microstrip antenna for communication with medical implants,” *IEEE*
 477 *Trans. Microw. Theory Tech.*, vol. 52, no. 8, pp. 1944–1951, Aug. 2004.
 478 [9] P. Soontornpipit, C. M. Furse, and Y. C. Chung, “Miniaturized biocompat- 478
 479 ible microstrip antenna using genetic algorithm,” *IEEE Trans. Antennas*
 480 *Propag.*, vol. 53, no. 6, pp. 1939–1945, Jun. 2005.
 481 [10] W.-C. Liu, F.-M. Yeh, and M. Ghavami, “Miniaturized implantable broad- 481
 482 band antenna for biotelemetry communication,” *Microw. Opt. Technol.*
 483 *Lett.*, vol. 50, pp. 2407–2409, Sep. 2008.
 484 [11] W.-C. Liu, S.-H. Chen, and C.-M. Wu, “Bandwidth enhancement and 484
 485 size reduction of an implantable PIFA antenna for biotelemetry devices,”
 486 *Microw. Opt. Technol. Lett.*, vol. 51, pp. 755–757, Mar. 2009.
 487 [12] C.-M. Lee, T.-C. Yo, and C.-H. Luo, “Compact broadband stacked im- 487
 488 plantable antenna for biotelemetry with medical devices,” in *Proc. IEEE*
 489 *Annu. Wireless Microw. Technol. Conf.*, Dec. 4–5, 2006, pp. 1–4.
 490 [13] A. Kiourti and K. S. Nikita, “Meandered versus spiral novel miniature 490
 491 PIFAs implanted in the human head: Tuning and performance,” presented
 492 at the 2nd ICST Int. Conf. Wireless Mobile Commun. Healthcare, Kos
 493 Island, Greece, 2011, to be published.
 494 [14] F. Merli and A. K. Skrivervik, “Design and measurement considerations 494
 495 for implantable antennas for telemetry applications,” in *Proc. 4th Europ.*
 496 *Conf. Antennas Propag.*, Barcelona, Spain, Apr. 2010, pp. 1–5.
 497 [15] F. Merli, L. Bolomey, J.-F. Zurcher, G. Corradini, E. Meurville, and 497
 498 A. K. Skrivervik, “Design, Realization and measurements of a minia-
 499 ture antenna for implantable wireless communication systems,” *IEEE*
 500 *Trans. Antennas Propag.*, vol. 59, no. 10, pp. 3544–3555, Oct. 2011.
 501 [16] W. Sun and Y.-X. Yuan, *Optimization theory and methods*. New York:
 502 Springer-Verlag, 2006, ch. 5.
 503 [17] A. Kiourti and K. S. Nikita, “Detuning issues and performance of a novel 503
 504 implantable antenna for telemetry applications,” presented at the 6th Eu-
 505 rop. Conf. Antennas Propag., Prague, Czech Republic, Mar. 2012.
 506 [18] W. G. Scanlon and J. B. Burns, “Radiowave propagation from a tissue- 506
 507 implanted source at 418 MHz and 916.5 MHz,” *IEEE Trans. Biomed.*
 508 *Eng.*, vol. 47, no. 4, pp. 527–534, Apr. 2000.
 509 [19] L. C. Chirwa, P. A. Hammond, S. Roy, and D. R. S. Cumming, “Electro- 509
 510 magnetic radiation from ingested sources in the human intestine between
 511 150 MHz and 1.2 GHz,” *IEEE Trans. Biomed. Eng.*, vol. 50, no. 4,
 512 pp. 484–492, Apr. 2003.
 513 [20] *Ansoft High Frequency Structure Simulator (HFSS)*, Ver. 11, Ansoft Cor- 513
 514 poration, Pittsburgh, PA, 2008.
 515 [21] *XFDTD®*, *Electromagnetic Solver Based on the Finite Difference Time*
 516 *Domain Method*, Remcom, Inc., State College, PA.
 517 [22] C. Gabriel, S. Gabriel, and E. Corthout, “The dielectric properties of 517
 518 biological tissues,” *Phys. Med. Biol.*, vol. 41, pp. 2231–2293, 1996.
 519 [23] A. Kiourti, M. Tsakalakis, and K. S. Nikita, “Parametric study and design 519
 520 of implantable PIFAs for wireless biotelemetry,” presented at the Proc.
 521 2nd ICST Int. Conf. Wireless Mobile Commun. Healthcare, Kos Island,
 522 Greece, 2011.

Q2

Q3

- 523 [24] D. Popovic, L. McCartney, C. Beasley, M. Lazebnik, M. Okoniewsky, 531
524 S. C. Hagness, and J. H. Booske, "Precision open-ended coaxial probes 532
525 for *in vivo* and *ex vivo* dielectric spectroscopy of biological tissues at 533
526 microwave frequencies," *IEEE Trans. Microw. Theory Tech.*, vol. 53, 534
527 no. 5, pp. 1713–1722, May 2005. 535
- 528 [25] R. Zajicek, L. Oppl, and J. Vrbaf, "Broadband measurement of complex 537
529 permittivity using reflection method and coaxial probes," *Radioengineer-* 538
530 *ing*, vol. 17, pp. 14–19, Apr. 2008.
- [26] A. Kiourti and K. S. Nikita, "Miniature scalp-implantable antennas for 531
telemetry in the MICS and ISM bands: Design, safety considerations and 532
link budget analysis," *IEEE Trans. Antennas Propag.*, to be published. 533
- [27] *IEEE Standard for Safety Levels with Respect to Human Exposure to 534
Radiofrequency Electromagnetic Fields, 3 kHz to 300 GHz*, IEEE Standard 535
C95.1-1999, 2005.
- Authors' photographs and biographies not available at the time of publication. 537
538

IEEE
Proof

QUERIES

- Q1. Author: Citation of “Fig.14” has been changed to “Fig. 13” in sentence “Local SAR . . . been recorded.” Please verify.
- Q2. Author: Please provide name of the authors in Refs. [6], [7].
- Q3. Author: Please provide the year information in Refs. [13], [21].
- Q4. Author: Please update Ref. [26].

539

540

541

542

543

IEEE
Proof